PROCEEDINGS OF SCIENCE

Modelling the γ-ray emission from η Carinae

Matteo Balbo and Roland Walter*

Department of Astronomy, University of Geneva, Chemin Pegasi 51, CH-1290 Versoix, Switzerland

E-mail: Matteo.Balbo@unige.ch, Roland.Walter@unige.ch

After the detection by the H.E.S.S. Cherenkov telescope of the very-high-energy γ rays coming from the colliding wind binary η Carinae, we explored the possibility that its spectral cut-off is not due to an intrinsic cut-off in the accelerated particle population, but rather being a feature arising from the γ-γ opacity. We developed a model which reproduces the expected γ-γ absorption between the very-high-energy γ rays interacting with the intense ultraviolet fields of both stars, assuming the two most likely orbital orientations. Thanks to its deep sensitivity, the Cherenkov Telescope Array (CTA) has the potential to exclude one of the two orientations detecting fast spectral variability on daily/weekly timescale, when at periastron the orbital positions of the two stars vary the most. It can also constrain the magnetic field and the spatial locations where particles are accelerated to their highest energy via diffusive shock acceleration. The eventual detection by CTA of a rising spectrum due to the Rayleigh-Taylor tail of the absorption will be the indisputable confirmation that colliding wind binaries can accelerate particles to energies larger than those one found in supernova remnants.

38th International Cosmic Ray Conference (ICRC2023)
26 July - 3 August, 2023
Nagoya, Japan

*Speaker

PoS(ICRC2023)909

1. Introduction

Colliding winds of massive stars in binary systems (CWB) have been proposed as potential sites of relativistic cosmic-ray acceleration and non-thermal very-high-energy (VHE) photons since more than 40 years [24]. In these systems, diffusive shock acceleration (DSA) provides high-energy (HE) particles out of a thermal pool [8]. Such relativistic particles subsequently cool down via different radiation processes, mostly inverse-Compton (IC) for leptons and photo-pion production for hadrons. This radiation has been detected in η Carinae, the archetype of CWB, from hard X-rays [20] up to several hundreds GeV [14]. In particular, VHE γ-rays can be absorbed interacting with the huge pool of thermal UV photons provided by one or both stars, creating electron-positron pairs, significantly modifying the γ-ray spectrum measured by the observer at Earth.

2. γ-ray obscuration

The presence of Wolf-Rayet (WR) stars in CWB systems, with their typically high luminosity, guarantee the existence of a large pool of thermal UV photons, that can interact with the γ-rays produced by the cooling of the wind-shocked accelerated particles. The interaction of a γ-ray of energy E_γ with a star photon of energy $\epsilon_\star$ can lead to the production of an electron-positron pair [25] if the threshold equation $E_\gamma \epsilon_\star \geq \frac{2m_e^2 c^4}{(1-\hat{\mathbf{e}}_\gamma \hat{\mathbf{e}}_\star)}$ is satisfied. Here $\hat{\mathbf{e}}_\gamma$ indicates the unit vector along the propagation of the γ-ray photon, whereas $\hat{\mathbf{e}}_\star$ is the one related to the star photon, m_e is the electron mass, and c is the speed of light. The collision angle among the two photons plays a very important role, and in some situations a simplistic head-on treatment can yield to strongly different results. For convenience of calculation, we use the same geometrical description and notation used by [7], and the total optical depth for a γ-ray of energy E_γ travelling toward the observer is:

$$\tau_{\gamma\gamma} = \int_0^\infty \mathrm{d}l \int_{c_{min}}^1 \mathrm{d}\cos\theta \int_0^{2\pi} \mathrm{d}\phi \int_{\epsilon_{min}}^\infty (1 - \hat{\mathbf{e}}_\gamma \cdot \hat{\mathbf{e}}_\star)\, n_\epsilon\, \sigma_{\gamma\gamma}\, \mathrm{d}\epsilon \tag{1}$$

where n_ϵ represents the classical blackbody radiation density of low-energy (LE) photons emitted from the primary star and $\sigma_{\gamma\gamma}$ is the cross section of the process $\gamma + \gamma \rightarrow e^+ + e^-$ [25]. Regarding the boundary of the quadruple integral, ϵ_{min} can be derived from the threshold equation, and $c_{min} = \sqrt{1 - R_\star^2/d^2}$ with $R_\star$ being the radius of the primary star and d its distance from the point where the optical depth is computed [7]. So in order to compute the exact probability that a HE γ-ray, produced in a wind-shocked binary system and travelling toward the observer, has to interact with the LE photons emitted by the primary star, we need to know the orientation of the binary system, the location where the HE γ-rays are produced, the star luminosities and the temperatures.

3. η Carinae's orbit

The η Carinae binary system is composed of one of the most luminous and massive star of our Galaxy, expected to be a luminous blue variable [6], and its companion, a late-type nitrogen-rich O or WR star [17]. The mass of the primary star is supposed to be larger than 90 $M_\odot$, while the secondary one is within 20 $\sim$ 50 $M_\odot$ [16, 23]. They both emit powerful stellar winds. The one from the primary star is denser but slower, with a mass-loss rate of nearly $\sim 10^{-3}\ M_\odot\ \mathrm{yr}^{-1}$ and a terminal wind velocity of $\sim 500\ \mathrm{km\ s}^{-1}$, whereas the one from the secondary star is faster but lighter, with a mass-loss rate of $\sim 10^{-5}\ M_\odot\ \mathrm{yr}^{-1}$ and a terminal wind velocity of $\sim 3000\ \mathrm{km\ s}^{-1}$. The system is located in the Carina arm of our Galaxy, at an estimated distance of 2.35 ± 0.05 kpc [26]. Recent

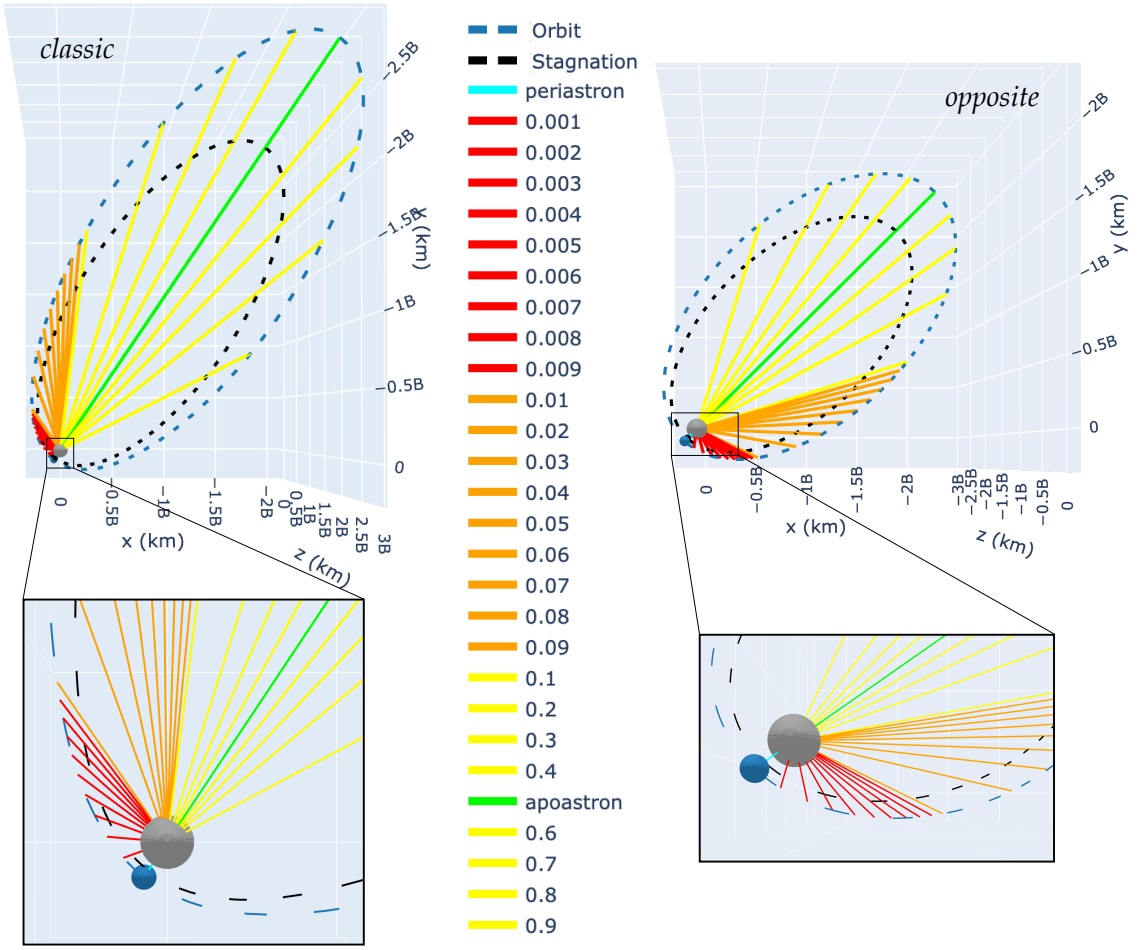

Figure 1: Orientation of the η Carinae orbit as seen from the Earth. The $\overrightarrow{\mathbf{xyz}}$ reference system is centered at the primary star position. The *z-axis*, coincident with our line of sight, is parallel to $\hat{\mathbf{e}}_\gamma$. Blue dashed and black dashed lines indicate the position of the secondary star and the stagnation point during the entire orbit, respectively. The various red, orange, and yellow lines, instead, are the separation vector that connect the two stars at the labelled phases. The inset at the bottom represents a zoom around periastron.

Gaia measurements proposed a possible increase of the distance by 10% [12]. The two stars are in a very eccentric orbit $e > 0.85$ [4], and the orbital period corresponds to 2022.7 ± 1.3 days [5]. The exact orientation of η Carinae's orbit still presents quite some uncertainties. The secondary star is not optically visible, due to its much fainter luminosity compared to the primary one and due to large quantity of dust surrounding the system. From observations at other wavelengths, the orientation of the orbital plane is suggested as nearly perpendicular to the polar axis of the Homunculous Nebula [21]. We report in Table 1 the orbital parameters we have used to orient η Carinae binary system with respect to the observer, in agreement with the work of [13]. The resulting 3D orbit, as seen from the line of sight of the observer is shown on the left of Figure 1. In particular, the secondary star is on the far side of the primary, with respect to our line of sight, only for a small period of the orbit at around periastron. Another possible orientation

Table 1: Simulated orbital elements.

η **Carinae**		
orientation	*classical*	*opposite*
ω (°)	263	90
i (°)	138	42
PA_z (°)	317	
e	0.93	
a (A.U.)	15.4	
P_{orb} (days)	2022.7 ± 1.3	
φ_0 (year)	2020.11	
distance (kpc)	2.3	

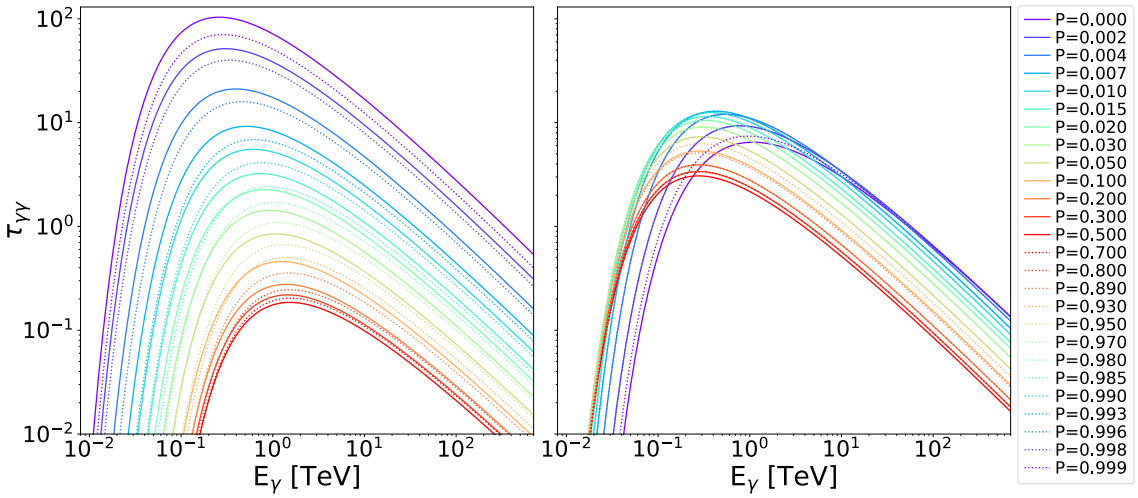

Figure 2: The plot shows the optical depth for γ-rays of energy E_γ from 1 GeV to 700 TeV, emitted close to the stagnation point, at various orbital phases. Solid lines indicate orbital phases from periastron to apastron, elsewhere dotted lines are used. The *left* (*right*) panel shows the result for the *classical* (*opposite*) orientation.

[18, 19] results in a nearly opposite configuration, reflected with respect to a plane orthogonal to the observer's line of sight (Figure 1, right). In such a configuration, the primary star is on the far side of the companion at periastron with respect to our line of sight. For convenience, hereafter we will denote the first described orientation as *classical*, and the last one as *opposite* (Table 1).

4. Models and simulations

When the supersonic winds of two stars collide they form a thin shell composed of two radiative shocks, which are in general separated by a contact discontinuity (CD). It is called *stagnation point* the position along the line connecting the two stars where the wind ram-pressure is in equilibrium. The square ratio of the stagnation point distances from the primary star (r_{s1}) and from the secondary star (r_{s2}) is $\frac{r_{s1}^2}{r_{s2}^2} = \frac{\dot{M}_{w1} v_{w1}}{\dot{M}_{w2} v_{w2}} \equiv \beta$, where $\dot{M}_{wi}$ and v_{wi} are the mass-loss rate and wind velocity for the i-th star. Substituting the values from the literature [3] we get $\beta \simeq 12 \sim 16$. In Figure 1 the black dashed lines indicate the stagnation point location during the whole orbit for $\beta = 12$, in both orientations, and Figure 2 reports the optical depth values for various orbital phases, assuming that HE γ-rays are produced in a very small region around the stagnation point. From considerations on the mass, the linear and the angular momentum conservation, we can derive the locus of points that satisfy the pressure equilibrium between the two winds. We use the algebraic solutions proposed by [2], rotated about the line joining the two stars, to describe the 3D shape of the thin CD surface arising from the collision of the two winds (Figure 3, green paraboloid). As can be seen from the simulations of [9], in the case of a simple adiabatic expansion, three distinct structures are produced: a shock front for each star, separated by a CD. We reproduce such structures using the same analytical solution used before, but with three different values of β which

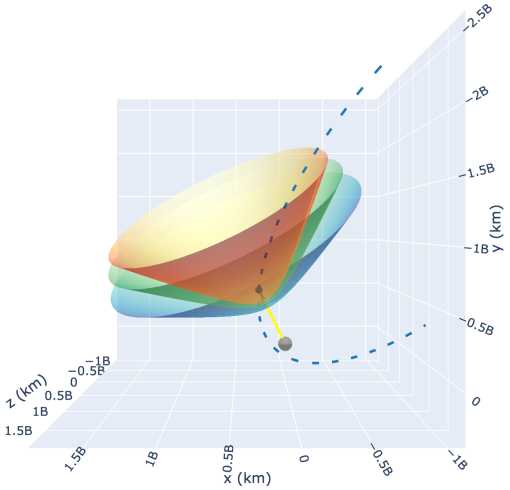

Figure 3: The 3D CD surface, derived from the 2D equations of [2], for a given orbital phase, are shown for three arbitrarily different values of the wind momentum ratio: $\beta = 9$ (blue), $\beta = 16$ (green), $\beta = 25$ (red).

change the opening angle (Figure 3). If instead we consider the presence of strong radiative cooling, the Rankine-Hugoniot jump conditions in the pre- and post-shock regions are significantly altered [10, 11]. Particles could lose their energies faster than the time needed to flow out from the shocked regions, reducing the total pressure within the shocked surface, and resulting in greater compression of the gas and thinning of the shocked layers, subject to thin-layer instabilities [9]. The final picture is more turbulent and the three different structures disappear in a chaotic vortex from the mixture of the two gases. The differences in the cone aperture from both sides of the stars are also smaller (see Figure 1 of [9]), and the intrinsic error due to a simplified single-paraboloid representation is largely reduced. Moreover, the magnetic energy is concentrated in filaments that are well distributed along the shocked region, in contrast to the simple adiabatic case where the magnetic energy was mainly concentrated around the apex, close to the stagnation point. Despite the shocked surfaces where particles are accelerated are not smooth and altered by the arising of turbulence, for what concern the optical depth the paraboloid approximation is still valid as we are just interested in the 3D spatial location of the shocks with respect to the observer. The final results clearly depend on the source function characterising the densities and the regions where HE γ-rays are emitted, but its parameterization remains largely unknown. We describe the HE γ-ray density over the 3D paraboloids as a function of distance from the primary star, proportional to d^{-1}, d^{-2} and d^{-3}, which should correlate with the intensity of a toroidal, radial, and dipolar magnetic field, respectively. We solve the transfer equation numerically over the entire thin paraboloidal surface, which is consistent with the case of pure absorption. We estimate the uncertainties we might introduce with the simple paraboloid approximation, considering the two extreme cases where all HE emissivity is entirely concentrated in the reverse shock on the side of the primary star or on the side of the companion (assuming $\beta_{1\star} < \beta_{CD} < \beta_{2\star}$). This lead to a variation of the maximum absorption by at most 10% in the *classical* orbital orientation, and less than 0.4% for the *opposite* one. If we assume instead that the HE γ-rays are generated over the entire volume bounded by the two extreme paraboloids the discrepancies are mitigated. The differences arising from the choice of orbital orientation or the physical extension of the paraboloid are larger than the uncertainties arising from the assumption of a single-paraboloid with a given β rather than a filled volume delimited by the two more extreme paraboloid cases. For this reason, in the following analysis we will consider a single thin paraboloid with an intermediate beta value, and a mass of 100 $M_\odot$, a radius of 100 $R_\odot$, a temperature of $T_1 = 2.6 \cdot 10^4$ K for the primary star, whereas the secondary is at least one order of magnitude less luminous and with a radius of 14 $R_\odot$.

5. Discussion

We compare our optical depth calculation with actual observed data by Fermi-LAT [22, 27] and H.E.S.S. [14]. The exposure of the Fermi-LAT data can be considered homogeneous over time, while the H.E.S.S. spectra are obtained from the stacking of different punctual observations. The latter data are therefore better suited for comparison with an optical depth estimated at a particular precise orbital phase, while the former data should be compared with an optical depth averaged over the same exposure time interval, bearing in mind that the intrinsic γ-ray spectrum may also vary across different orbital phases. The LE turning of the Fermi-LAT data at around $\sim$ 1 GeV cannot be explained as an apparent feature caused by the γ-γ absorption, since this would require an unphysically high surface temperature for the stars. The H.E.S.S. data from orbital phase

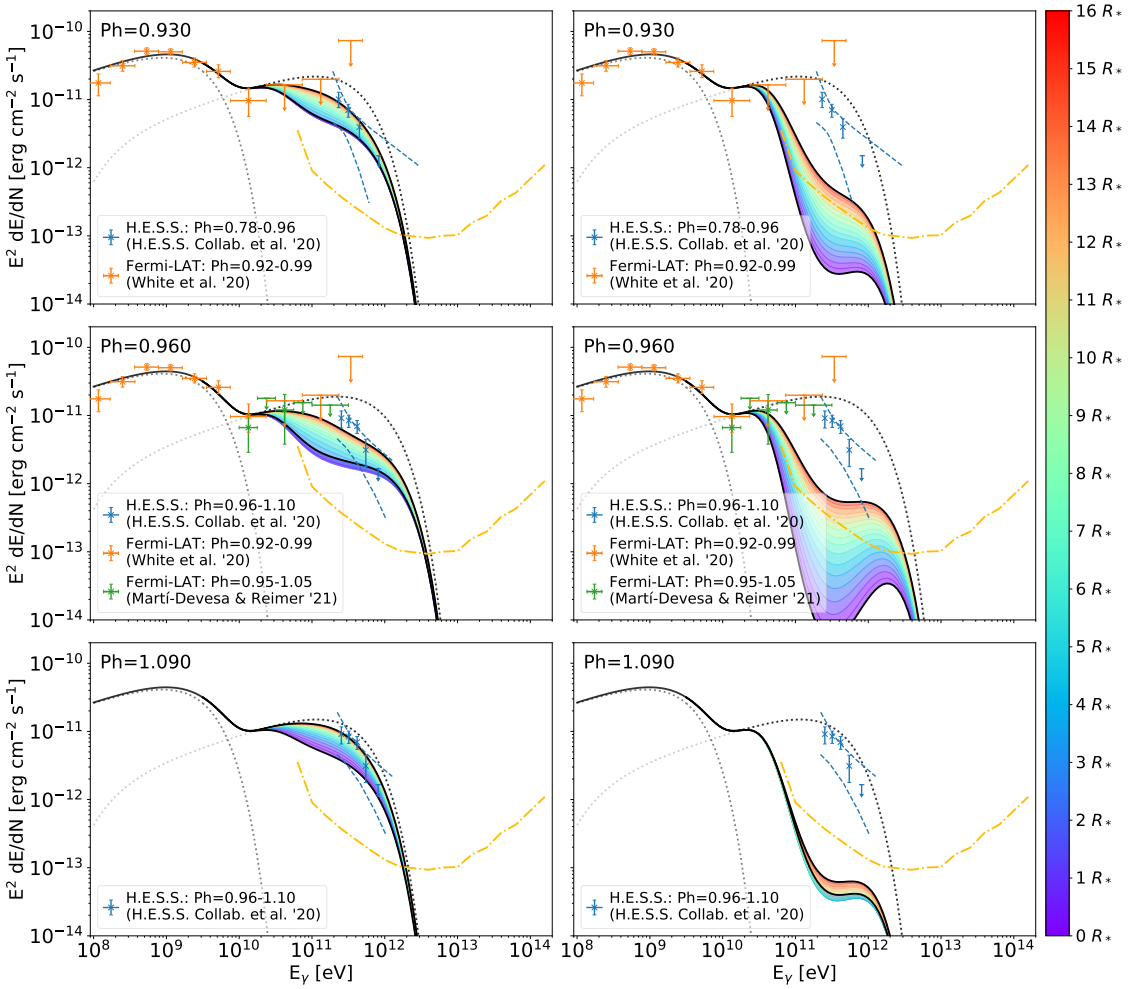

Figure 4: Expected γ-γ absorption by the primary and secondary stars at different orbital phases. A PLEC with photon index -1.65 [15] and 2.5 GeV energy cutoff are plotted over the LE Fermi-LAT data. Another PLEC with the same photon index and different energy cutoffs (from $\sim$ 300 to $\sim$ 650 GeV) are superimposed to the HE data. The dotted lines indicate the intrinsic spectra, while the filled regions represent the absorbed spectra, with HE γ-rays density $\propto d^{-2}$ from the primary star, and with different colours as a function of paraboloid extension. The yellow dot-dashed line represents the publicly available CTA "Alpha Configuration" 50 h CTA sensitivity[1] at 20° from zenith. Both *classical* (left) and *opposite* (right) orientation are simulated. Fermi-LAT and H.E.S.S. data refer to the same periastron passage occurred in 2014.

0.78-0.96 are likely dominated by the very long observation at phase 0.93. We have assumed in Figure 4 an arbitrary intrinsic power-law with exponential cutoff (PLEC) spectrum convolved with the simulated optical depth in those orbital phases where H.E.S.S. performed its longest observations. When available, we also included for reference the Fermi-LAT data whose time interval is compatible with the orbital phase of the H.E.S.S. observations. We simulated both system orientations and assumed for simplicity that HE γ-rays have the same spectral properties over the entire small paraboloid surface, with its density scaled $\propto d^{-2}$. Providing that the assumed values for the radius and temperature of both stars are correct, at orbital phase 0.93 the single stagnation point approximation almost reproduce the data, while a single small paraboloid better fits them. In addition, assuming that the two shocked regions accelerate two independent populations

[1]The CTA instrument response function (prod5 v0.1) provided by the CTA Consortium and Observatory (https://www.cta-observatory.org/science/cta-performance) does not account for the bright optical background of the Carina region which will need to be taken into account in the spectral extraction.

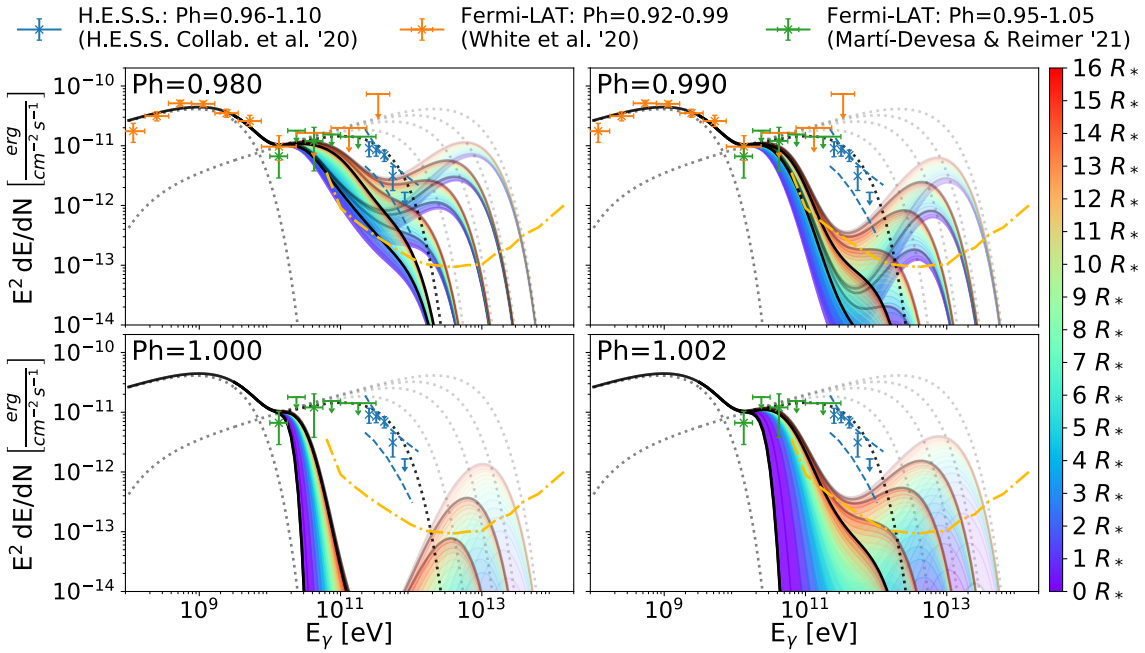

Figure 5: Simulated temporal evolution of the optical depth during the orbital phase 0.98-1.002. We assumed a constant intrinsic γ-ray spectrum during this interval and we overplotted the results for arbitrarily larger cutoff energies with faded colors (0.3, 0.6, 1.5, 3, and 6 TeV). The optical depth takes into account the contributions of both stars, and a density of HE γ-rays $\propto d^{-2}$ is assumed over a thin paraboloid surface. The results are for the *classical* orientation. For the sake of comparison, the same Fermi-LAT and H.E.S.S. data of the previous figures and the CTA sensitivity are overplotted. The reported H.E.S.S. data were taken exactly at orbital phase 0.96, 1.09 and 1.10.

of particles, would also allow to fit the LE Fermi-LAT data, without being much affected by the convolution with the simulated optical depth, in agreement with our previous work [1] or with a soft population of hadrons with photon index $\Gamma \lesssim -2.5$. At phase 0.96, the H.E.S.S. data cannot be reproduced by the single stagnation point model, while can be fitted by a paraboloid (extended up to $\sim 50\ R_\star$). If we instead reduce the assumed luminosity of the secondary star, or ignoring completely its contribution, the convolved results converge toward the intrinsic spectrum. After periastron, there are no Fermi-LAT data available from [22, 27] compatible with orbital phase 1.09. Nevertheless, keeping the same specatral parameters used before, convolved with the appropriate simulated optical depth, the H.E.S.S. data are almost compatible with the single stagnation point model and even better reproduced by the small paraboloid one. Similarly to before, a reduction in the secondary star luminosity will significantly reduce the optical depth and shift it toward higher energies. Interestingly, if we instead assume the *opposite* orientation of the system (see right column of Figure 4), the simulated convolved spectra are not compatible with the H.E.S.S. data at any orbital phase, neither with the stagnation point approximation nor with the paraboloid one, regardless the shape of the assumed intrinsic γ-ray spectra. The only way to make the data consistent with the paraboloid model would be to assume that the HE γ-rays are generated extremely far from the stagnation point ($d \gg 10^{15}$ cm), where the optical depth becomes negligible and the simulated spectra are very close to the intrinsic ones. But this physical situation seems unlikely. Reducing or ignoring the luminosity of the secondary star is also not helpful, since it affects the final optical depth only near the periastron (within orbital phase $0.995 \sim 1.007$). In all other orbital phases, the absorption is dominated by the contribution of the primary star.

Current H.E.S.S. data constrains the maximum γ-ray energy cutoff below $\sim$ 1 TeV. But there

are no published observations between phase 0.96 and 1.1 (see Figure 4 of [14]). So an intrinsic larger cutoff, when the system conditions are more extreme is still not ruled out, and paradoxically a non-detection by H.E.S.S. around periastron passage would still not rule out this option, as visible from Figure 5. Indeed, assuming the *classical* orientation, will be easier to satisfy an hypothetical H.E.S.S. UL at around periastron than to fit an H.E.S.S. detection, since the absorption feature is maximised exactly around its energy band. Only simultaneous CTA observations at LE and VHE band will decree a final judgement on the maximum cutoff energy.

6. Conclusion

In this work we calculate the probability of interactions of VHE γ-rays with thermal photons from both non-pointlike stars in the η Carinae binary system, assuming the two most likely orbital orientations, and potentially excluding one of them, which predicts too high an absorption to be compatible with the Fermi-LAT and H.E.S.S. data. A modulation of the absorption along the entire orbit is expected, due to the change in the relative position between the shocked regions and the stars with respect to the observer. We predict also a strong variability at around periastron and the necessity of simultaneous CTA observations at LE and VHE to unequivocally determine the maximum γ-ray energy cutoff, which is critical for estimating the maximum energy that particles can reach in wind-shocked systems, and potentially shedding more light on other parameters of the system (eccentricity, radii, temperatures, magnetic field of the stars, and wind-shocked locations).

References

[1] Balbo M., Walter R., 2017, A&A, 603, A111
[2] Canto J., Raga A. C., Wilkin F. P., 1996, ApJ, 469, 729
[3] Corcoran M. F., Hamaguchi K., 2007, in Proceedings. pp 29–34 (arXiv:astro-ph/0703039)
[4] Damineli A., Conti P. S., Lopes D. F., 1997, New A, 2, 107
[5] Damineli A., et al., 2008, MNRAS, 384, 1649
[6] Davidson K., Humphreys R. M., 1997, ARA&A, 35, 1
[7] Dubus G., 2006, A&A, 451, 9
[8] Eichler D., Usov V., 1993, ApJ, 402, 271
[9] Falceta-Gonçalves D., Abraham Z., 2012, MNRAS, 423, 1562
[10] Falceta-Gonçalves D., Jatenco-Pereira V., Abraham Z., 2005, MNRAS, 357, 895
[11] Falceta-Goncalves D., 2015, in Proceedings. pp 289–292 (arXiv:1510.06106)
[12] Gaia Collaboration et al., 2018, A&A, 616, A1
[13] Groh J. H., Hillier D. J., Madura T. I., Weigelt G., 2012, MNRAS, 423, 1623
[14] H. E. S. S. Collaboration et al., 2020, A&A, 635, A167
[15] Hamaguchi K., et al., 2018, Nature Astronomy, 2, 731
[16] Hillier D. J., Davidson K., Ishibashi K., Gull T., 2001, ApJ, 553, 837
[17] Iping R. C., Sonneborn G., Gull T. R., Massa D. L., Hillier D. J., 2005, ApJ, 633, L37
[18] Kashi A., Soker N., 2016, ApJ, 825, 105
[19] Kashi A., Principe D. A., Soker N., Kastner J. H., 2021, ApJ, 914, 47
[20] Leyder J. C., Walter R., Rauw G., 2008, A&A, 477, L29
[21] Madura T. I., Gull T. R., Owocki S. P., Groh J. H., Okazaki A. T., et al. 2012, MNRAS, 420, 2064
[22] Martí-Devesa G., Reimer O., 2021, A&A, 654, A44
[23] Mehner A., Davidson K., Ferland G. J., Humphreys R. M., 2010, ApJ, 710, 729
[24] Montmerle T., 1979, ApJ, 231, 95
[25] Nikishov A. I., 1962, , 14, 393
[26] Smith N., 2006, ApJ, 644, 1151
[27] White R., Breuhaus M., Konno R., Ohm S., Reville B., Hinton J. A., 2020, A&A, 635, A144